American Mineralogist, Volume 97, pages 807–815, 2012

Wassonite: A new titanium monosulfide mineral in the Yamato 691 enstatite chondrite

Keiko Nakamura-Messenger,[1,2,*] Simon J. Clemett,[2,3] Alan E. Rubin,[4] Byeon-Gak Choi,[5] Shouliang Zhang,[2,6,7] Zia Rahman,[1,2] Katsunari Oikawa,[8] and Lindsay P. Keller[2]

[1]ESCG/Jacobs Technology, Texas 77058, U.S.A.
[2]Robert M Walker Laboratory for Space Science, Astromaterials Research and Exploration Science Directorate/NASA Johnson Space Center, Houston, Texas 77058, U.S.A.
[3]ESCG/ERC Inc., Texas 77058, U.S.A.
[4]Institute of Geophysics and Planetary Physics, University of California, Los Angeles, California 90095-1567, U.S.A.
[5]Earth Science Education, Seoul National University, Seoul 151-748, South Korea
[6]Lunar and Planetary Institute, Houston, Texas 77058, U.S.A.
[7]Texas Material Institute, University of Texas, Austin, Texas 78712, U.S.A.
[8]Department of Metallurgy, Graduate School of Engineering, Tohoku University, Sendai, 980-8579, Japan

Abstract

Wassonite, ideally stoichiometric TiS, is a titanium monosulfide not previously observed in nature, that was discovered within the Yamato 691 EH3 enstatite chondrite. Twelve Ti-S phase grains were identified in a rare barred olivine (BO) chondrule; three of the grains were extracted by the focused ion beam technique. Because of the submicrometer size of the wassonite grains, it was not possible to determine conventional macroscopic properties. However, the chemical composition and crystal structure were well constrained by extensive quantitative energy-dispersive X-ray analysis and electron diffraction using transmission electron microscopy (TEM). The crystal system for wassonite is rhombohedral ($a = 3.42 \pm 0.07$, $c = 26.50 \pm 0.53$ Å) with space group: $R\bar{3}m$, cell volume: 268.4 ± 0.53 Å^3, $Z = 9$, density (calculated): 4.452 g/cm^3, empirical formula: $(Ti_{0.93},Fe_{0.06},Cr_{0.01})S$. The wassonite grains crystallized from the chondrule melt that was itself formed in the solar nebula, not on the parent asteroid. The other crystalline phases in the BO chondrule include forsterite, enstatite, troilite, metallic Fe-Ni, and osbornite (as well as the new Ti-S-bearing minerals and schollhornite) are highly reduced and indicate formation at low-oxygen fugacities.

Keywords: New mineral, wassonite, TiS, Antarctic meteorite, TEM, electron diffraction

Introduction

The inland traverse party of the tenth Japanese Antarctic Research Expedition (JARE-10) found, by accident, nine meteorites on the ice including the Yamato A meteorite (later renamed Yamato 691) in December 1969. Initially, these nine samples were thought to be pieces of a single meteorite, but later investigations revealed that they represented several different meteorite types: an EH3 enstatite chondrite (Yamato 691), a CK4/5 carbonaceous chondrite, a diogenite (orthopyroxenite), and six equilibrated H-group ordinary chondrites (some of which could be paired). This surprising diversity led to follow-up systematic searches for meteorites in Antarctica (Kojima 2006). These international searches have successfully recovered more than 40 000 total specimens (and still counting), including martian meteorites, lunar meteorites, and several rocks derived from previously unsampled asteroids.

Yamato 691 was discovered in 1969, the same historic year as the falls of the landmark CV3 Allende and CM2 Murchison carbonaceous chondrites and the return of lunar samples from the Apollo 11 and 12 missions. These samples are among the most important extraterrestrial geological materials ever recovered, and their study has revolutionized our understanding of the formation and history of the solar system.

Yamato 691 (Y 691) is an EH chondrite of low-metamorphic grade (petrologic type 3), thought to have been derived from an asteroid that probably formed in the inner solar system; this conclusion is based on the similarities between enstatite chondrites and the Earth in their O-, Cr-, Ni-, and Ti-isotopic compositions (Clayton et al. 1984; Trinquier et al. 2007, 2009; Regelous et al. 2008). Although the specific parent asteroid of the meteorite is not known, enstatite chondrites have been potentially linked to E-type asteroids (Gaffey and Kelley 2004). The enstatite chondrites are divided into two groups: EH (high total iron) and EL (low total iron), presumably derived from two separate asteroids. The EH chondrites are more reduced than EL, e.g., they contain higher concentrations of Si in kamacite (~3 wt% vs. ~1 wt%; Keil 1968). Although some sulfide phases (e.g., troilite, oldhamite) are common to EH and EL chondrites, there are differences in other sulfides; niningerite occurs exclusively in EH chondrites and ferroan alabandite in EL chondrites (Keil 1968). The two groups also differ in mean chondrule size (220 and 550 μm, respectively; Rubin 2000).

Enstatite chondrites are relatively rare, constituting only about 1.5% of observed meteorite falls (Weisberg et al. 2006).

* E-mail: keiko.nakamura-1@nasa.gov

0003-004X/12/0506–807$05.00/DOI: http://dx.doi.org/10.2138/am.2012.3946

They formed under highly reducing conditions in the solar nebula, as recorded by their mineralogy, mineral chemistry, and modal mineral abundances (e.g., Keil 1968). They contain high modal abundances of the mineral enstatite (with ~0.02–0.04 mol% Fs; Wasson et al. 1994), from which they derive their name. They also contain graphite, Si-rich metallic Fe, high modal abundances of kamacite (~20–25 wt%), and abundant sulfides (~10 wt%) (Keil 1968). The sulfides contain elements that are mainly lithophile under more oxidizing conditions: e.g., oldhamite (CaS), niningerite (Mg,Fe)S, ferroan alabandite (Mn,Fe)S, daubréelite ($FeCr_2S_4$), caswellsiliverite ($NaCrS_2$), and Ti-bearing troilite (FeS).

Here we describe the titanium monosulfide phase, a simple two-element mineral phase with a unique crystal structure that was approved as a new mineral by the International Mineralogical Association (IMA) in Feburary 2011.

The mineral is named in honor of John Taylor Wasson (b. 1934), professor from the University of California Los Angeles (UCLA) in the Departments of Chemistry and Biochemistry, and Earth and Space Sciences. He is also a member of the Institute of Geophysics and Planetary Physics. Wasson is known for achievements across a broad swath of meteorite and impact research including the use of precise neutron activation data to classify iron meteorites and chondritic meteorites and to formulate models for the observed chemical fractionations in bulk chondrites. He has used chemical, petrographic, and isotopic techniques to constrain the formation of chondrules and is a leader in the investigation of potential mechanisms for forming tektites. Wasson has given his permission for the phase to be named after him.

Samples, sample preparation, and experimental techniques

Samples

The Y 691 enstatite chondrite was collected as a single 715-g stone by the inland traverse party of JARE-10 in Antarctica on December 21, 1969. It was found on bare ice at the southeastern end of the Yamato Mountains, 300 km SW of the Japanese Showa Station in Antarctica (Kojima 2006) at 71°50′55″S 36°15′10″E (Grossman 2005). Wassonite occurs within a 72-µm diameter barred olivine (BO) chondrule in petrographic thin section 79-1 of the Y 691 EH3 chondrite. A search for additional wassonite grains in the thin section outside the BO chondrule was unsuccessful. The thin section belongs to the National Institute of Polar Research (NIPR) in Japan.

Minerals observed previously within the Y 691 meteorite include kamacite, perryite, schreibersite, troilite, daubréelite, niningerite, oldhamite, sphalerite, djerfisherite, caswellsilverite, graphite, roedderite, albite, enstatite, diopside, and forsterite (El Goresy et al. 1988; Ikeda 1989; Rubin et al. 2009). Mineralogical data for Y 691 from the NIPR Japan Antarctic Meteorites Database show the following mineral ranges (in mol%): olivine: 0.01–2.5% Fa; enstatite: 0.3–20.2% Fs; and plagioclase: 32–75% An.

Sample preparation

Twelve Ti-S phase grains (wassonite candidate grains) were indentified in the BO chondrule in the Y 691,79-1 thin section using the JEOL JXA-8200 electron microprobe at UCLA (Fig. 1). Mineral compositions were determined using natural standards (albite for Na; forsterite for Si and Mg; grossular for Al and Ca; orthoclase for K; sphene for Ti; chromite for Cr; Mn-rich garnet for Mn; and magnetite for Fe), an accelerating voltage of 15 keV, a 15 nA sample current, 20 s counting times, and ZAF corrections.

We used an FEI Quanta 3D 600 focused ion beam (FIB) instrument at the NASA Johnson Space Center (JSC) to extract, in situ, a cross section of the BO chondrule including two Ti-S grains (Fig. 1). The FIB section was prepared using a 30 keV focused Ga ion beam. Approximately 3-µm thick C- and Pt-strips were deposited to protect the region of interest (ROI) during the ion-beam milling. The 5×10 µm section was extracted and then attached to an OMNI half TEM grid with C and Pt deposition. After mounting on the TEM grid, the section was thinned down to a 50 nm thickness using 5 keV and finally 2 keV Ga+. This thinning process unfortunately sputtered out one of the TiS grains, but the other remained and was later identified as wassonite grain 1 in the series of TEM analyses.

Experimental techniques

Imaging and selected-area electron diffraction (SAED) were performed using JEOL 2500SE field-emission scanning TEM (FE-STEM) at JSC. The FE-STEM is equipped with a 50 mm^2 thin-window energy-dispersive X-ray spectrometer (EDS), and a Gatan Tridiem imaging filter (GIF). Bulk chemical compositions were measured using EDS as well as quantitative nanoscale elemental mapping (spectrum images). Spectrum images contain a high-count EDS spectrum in each pixel, enabling the determination of quantitative element abundances in addition to displaying the spatial distribution of major and minor elements. For the spectrum imaging, we raster scanned a 4-nm diameter incident probe (9 nA) with a dwell time of 50 µs/pixel to avoid beam damage and element diffusion during the experiment. The size of the scanned area was typically 256×204 pixels at a magnification that was optimized to limit over- or under-sampling with the 4 nm probe. A ROI was defined within the periphery of the wassonite grain in the FIB section and the EDS spectra in each pixel of the ROI were co-added to obtain the bulk composition of the grain. EDS spectra were quantified using standard Cliff-Lorimer thin-film analysis techniques combined with experimentally determined k-factors obtained from well-characterized standards (Cliff and Lorimer 1975). EDS spectra were collected so that counting statistical errors were 1% or less for major elements.

Electron energy loss spectra (EELS) for the C *K*, N *K*, O *K*, K $L_{2,3}$, and Ti $L_{2,3}$ edges were obtained with the GIF on wassonite grain 1. EELS data were acquired in the FE-STEM spot mode using a 4 nm probe with a nominal energy dispersion of 0.1 eV/channel. The energy resolution was 0.63 eV with an emission current of ~100 µA. Digital Micrograph (ver. 1.70.16) was used for FE-STEM-EELS data acquisition and processing. The application of the EELS technique to this study has a twofold advantage. First, it helps to verify if there is carbon, nitrogen, or oxygen in addition to titanium and sulfur in the new mineral. In X-ray analysis, the N*K*α X-ray is strongly absorbed by the polymer-based thin windows in the EDS detector, and the position of the oxygen K peak overlaps with that of the titanium

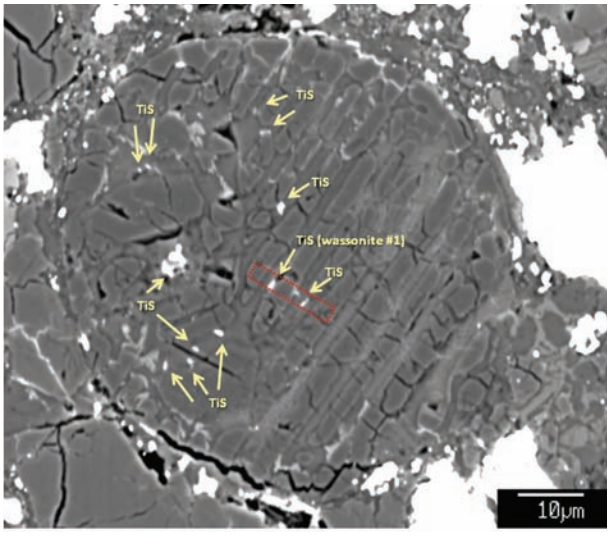

Figure 1. Location of the wassonite candidate grains within the BO chondrule in a petrologic thin section of Y-691. A BSE image of the wassonite-containing BO chondrule. The wassonite candidate (chemically TiS) is indicated with yellow arrows. A red broken line including two wassonite candidate grains is the targeted area of FIB extraction. Chemical compositions of the barred olivine grains and mesostasis are given in Table 1. Note that all the TiS grains were embedded in mesostasis; some of them were attached to the sides of the olivine bars.

L peak. Second, the titanium valence in the new mineral can be determined by comparing its Ti $L_{2,3}$ energy loss near edge structure with those from the reference materials with known Ti valence. Ilmenite, tistarite, and TiO were selected as references for Ti^{4+}, Ti^{3+}, and Ti^{2+} valences, respectively. All of the spectra were processed by power-law background subtraction followed by removal of plural scattering using low-loss region.

Interplanar spacings were measured from the SAED patterns and calibrated against a Au standard. The measured *d*-value error is ±0.04 Å. The values of camera length were calibrated at the same accelerating voltage and objective lens setting using an evaporated Au standard. For the SAED computer simulation, we used CrystalMaker-SingleCrystal software version 2.0.1 (Palmer 2005, SingleCrystal). We calculated the X-ray powder diffraction (XRD) pattern for wassonite using the XPOW program (Downs et al. 1993).

RESULTS

General mineralogy of the TiS-containing BO chondrule

Major phases of the wassonite-containing BO chondrule include olivine (Fa 0.7) and a feldspathic, moderately sodic mesostasis. Mean normalized compositions of olivine and mesostasis in the barred olivine chondrule are given in Table 1. Twelve Ti-S phase grains (wassonite candidate grains) were identified in the BO chondrule using the UCLA electron microprobe. All Ti-S phase grains were less than 0.5 µm in diameter. Despite a search, no other Ti-S grains were located in the thin section. All of the wassonite candidate grains occur within the mesostasis of the BO chondrule (Fig. 1).

Wassonite occurrence

In the FE-STEM observations of the FIB section (Fig. 2a), we identified that a wassonite grain (50 × 450 nm in size, hereafter wassonite grain 1) was cutting through the middle of an unknown Ti-rich layer phase, which has approximately the same cell parameters as schöllhornite (*a* = 3.32, *c* = 26.6 Å, $Na_{0.3}CrS_2 \cdot H_2O$) and wassonite (*a* = 3.4, *c* = 26.6 Å). Attached to one side of this assemblage, schöllhornite and another unknown phase occur (the unknown phase has a different composition but the same cell parameters as schöllhornite). Wassonite grain 1 formed within the mesostasis, but one side of it is attached to an olivine bar. Minor phases in the FIB section are enstatite, troilite, Fe-Ni alloy, osbornite, schöllhornite, and two unknown titanium-sulfide phases in the mesostasis. All of the minerals associated with wassonite grain 1 are illustrated in Figure 2b.

Chemical composition of wassonite

EDS analysis. A series of nanoscale elemental X-ray maps (Fig. 3) clearly show that only the core area, where wassonite grain 1 is located, is enriched in Ti and S and depleted in O, Ca, Cr, Mn, and Fe. Based on these quantitative EDS mappings, the major elements of wassonite are (in wt%): Ti 52.0, S 40.2, with minor Fe 4.0, Cr 0.47, Ni 0.31, and Ca 0.05. The elemental compositions for five points of wassonite grain 1 are summarized in Table 2.

TABLE 1. Mean normalized compositions (wt%) of olivine and mesostasis in the barred olivine chondrule

	Olivine	Mesostasis
SiO_2	42.8	69.2
TiO_2	0.09	0.1
Al_2O_3	0.16	20.6
Cr_2O_3	0.22	<0.04
FeO	0.67	0.35
MnO	0.05	<0.04
MgO	55.8	3
CaO	0.2	0.32
Na_2O	<0.04	6
K_2O	<0.04	0.51
Total	100	100.1
Fa	0.67	

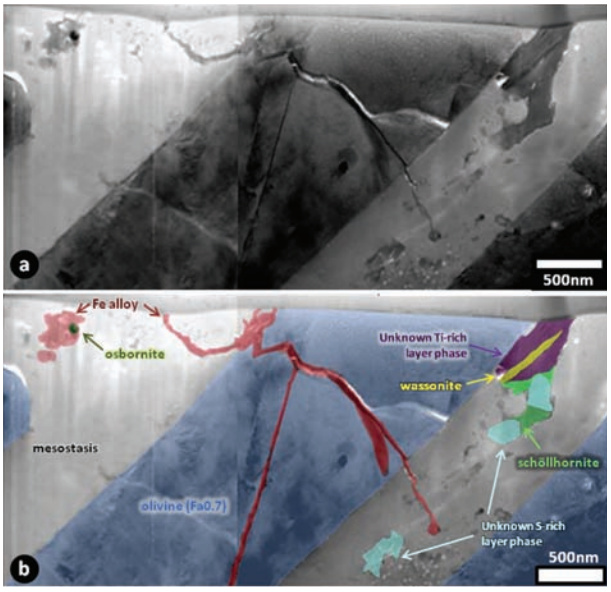

FIGURE 2. Associated minerals with wassonite in the FIB section from the BO chondrule in Y 691. (**a**) A mosaic of bright field STEM micrographs of the entire FIB section. (**b**) Mineral distribution image generated from the X-ray spectral mappings superimposed over **a**.

EELS analysis. The EELS data for C, N, and O show that these elements are below detection limits (<1 at%) in wassonite grain 1 (Fig. 4a), thus excluding the presence of Ti-nitride or Ti-oxide in the grain. Compared to the reference materials, the Ti $L_{2,3}$-edge structure of wassonite grain 1 is consistent with only the presence of Ti^{2+}.

The empirical formula of the new mineral is $(Ti_{0.93},Fe_{0.06},Cr_{0.01})S$. Cations were grouped in the proposed formula based upon the stoichiometry of synthetic sulfides. This can be abbreviated by the simplified formula Ti_1S_1, which requires Ti 59.88, S 40.12, for a total of 100.00 wt%.

Crystal structure of wassonite

Dark-field STEM imaging, high-resolution imaging (Fig. 5) and the SAED pattern reveal that wassonite grain 1 is a single domain crystal. We obtained SAED patterns from nine different zone axes (four major axes are shown in Fig. 6). The stereo projection is given as Appendix 1 from wassonite grain 1, allowing us to constrain the crystal structure of the TiS. Interplanar spacings measured from the SAED patterns and calculated *d*-spacings are displayed in Table 3 and compared to those for synthetic Ti-S cell parameters. We used the experimental SAED cell constants in the calculation of the powder X-ray diffraction pattern employing the XPOW program (Downs et al. 1993). The four most intense reflections are at *d* = 2.208 (*I* = 99.8), 1.71

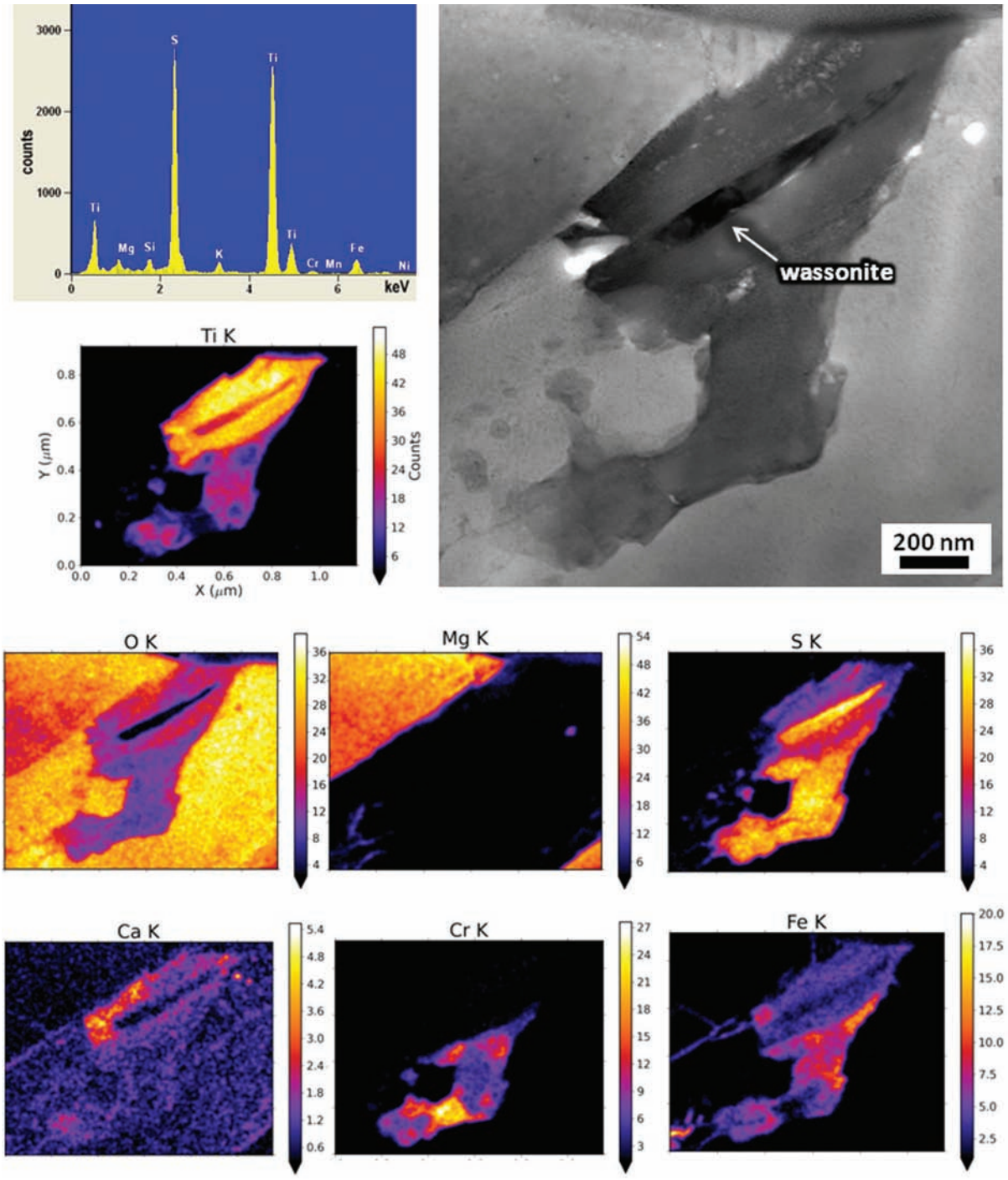

FIGURE 3. Wassonite elemental X-ray mapping. A bright-field STEM micrograph (right) showing wassonite grain 1 in dark contrast. EDS spectra of wassonite grain 1 is shown at left. Series of nanoscale elemental X-ray (*k*-line) maps of the same region show that wassonite grain 1 is chemically uniform but the surrounding material has various compositional differences.

(54.8), 2.59 (45.2), and 2.94 (36.0) (Table 4). The crystal structure and *d*-spacings of the new mineral (space group $R\bar{3}m$, $a = 3.42 \pm 0.07$, $c = 26.50 \pm 0.53$ Å, Fig. 7) are in excellent agreement with diffraction data for synthetic TiS of the rhombohedral system (Harn and Harder 1956).

Wassonite (low-*T* R9-type TiS) vs. high-*T* NiAs-type TiS

In synthetic titanium sulfides (Ti_xS_y), *x* and *y* take various values, and the crystal structure changes, depending on *x* and *y*; however, only TiS and Ti_8S_9 assume these elongated ($a = 3.42$, $c = 26.5$ Å) unit cells. TiS can crystallize in two polymorphs: the TiS

with space group $R\bar{3}m$ that we discovered in Yamato 691 is sometimes referred to as the "R9-type" in literature studies of synthetic Ti-S, in contrast to the nominal NiAs/B8-type crystal structure.

In synthetic (Fe,Ti)S monosulfide studies, the NiAs structure is observed in a composition region from pure FeS to $(Fe_{0.4}Ti_{0.6})S$ and pure TiS, whereas high-Ti content (Ti>Fe)S phases have the R9 structure (Nolze and Kraus 1998). The *a*- and *c*-axis of the NiAs structure monotonically increases and decreases with increasing TiS content, respectively (Mitsui 2009). The R9 structure phase is a NiAs-type superstructure transformed from the NiAs structure phase during the cooling, and the phase transformation from the NiAs-type to the R9-type is very sensitive

TABLE 2. Quantitative EDS spectral analyses (top: at%, bottom: wt%) of wassonite grain no. 1

Analysis		1	2	3	4	5
at% corrected for experimental k-factors (normalized)						
	Na	0.65	0.00	0.07	0.00	0.06
	O	0.00	0.00	0.00	0.00	0.00
	Mg	0.01	0.00	0.13	0.04	0.43
	Al	0.00	0.00	0.05	0.02	0.07
	Si	1.5	1.3	2.0	1.9	1.8
	S	51.3	49.5	49.1	49.1	48.8
	K	2.1	1.8	1.9	2.1	1.9
	Ca	0.05	0.03	0.03	0.12	0.00
	Ti	41.2	42.9	43.2	43.4	44.4
	Cr	0.43	0.47	0.36	0.33	0.21
	Mn	0.00	0.00	0.00	0.00	0.00
	Fe	2.7	3.0	3.2	2.9	2.4
	Ni	0.03	0.94	0.01	0.05	0.02
	Total	100.0	100.0	100.0	100.0	100.0
(Ca+Ti+Cr+Mn+Fe+Ni)/S		0.90	1.00	1.00	1.00	1.00
Ca/(Ca+Ti+Cr+Mn+Fe+Ni)		0.00	0.00	0.00	0.00	0.00
Ti/(Ca+Ti+Cr+Mn+Fe+Ni)		0.93	0.91	0.92	0.93	0.94
Cr/(Ca+Ti+Cr+Mn+Fe+Ni)		0.01	0.01	0.01	0.01	0.00
Mn/(Ca+Ti+Cr+Mn+Fe+Ni)		0.00	0.00	0.00	0.00	0.00
Fe/(Ca+Ti+Cr+Mn+Fe+Ni)		0.06	0.06	0.07	0.06	0.05
Ni/(Ca+Ti+Cr+Mn+Fe+Ni)		0.00	0.02	0.00	0.00	0.00
Analysis		1	2	3	4	5
wt% converted from at% (normalized)						
	Na	0.38	0.00	0.04	0.00	0.04
	O	0.00	0.00	0.00	0.00	0.00
	Mg	0.00	0.00	0.08	0.02	0.26
	Al	0.00	0.00	0.04	0.02	0.05
	Si	1.1	0.9	1.4	1.4	1.3
	S	42.0	40.3	39.6	39.6	39.4
	K	2.1	1.8	1.9	2.1	1.9
	Ca	0.05	0.03	0.03	0.12	0.00
	Ti	50.3	52.1	52.0	52.3	53.5
	Cr	0.57	0.62	0.47	0.43	0.28
	Mn	0.00	0.00	0.00	0.00	0.00
	Fe	3.9	4.2	4.5	4.1	3.3
	Ni	0.05	1.40	0.02	0.08	0.03
	Total	100.0	100.0	100.0	100.0	100.0

TABLE 3. Interplanar spacings measured from the SAED patterns of wassonite shown in Figure 8 and calculated *d*-spacings from TiS using the XPOW program (Downs et al. 1993)

h	*k*	*l*	*d* (Å) measured	*d* (Å) calculated
0	0	3	8.8208	8.8333
1	0	$\bar{1}$	2.9381	2.9435
1	0	$\bar{5}$	2.5792	2.5855
0	1	8	2.2003	2.2078
1	0	13	1.6646	1.6788
3	$\bar{1}$	1	1.1130	1.1185

TABLE 4. Calculated powder X-ray diffraction pattern for wassonite using the XPOW program (Downs et al. 1993)

2θ	Intensity	*d*-spacing	*h k l*
10.01	9.61	8.8333	0 0 3
30.36	4.63	2.9444	0 0 9
30.37	**36.01**	**2.9435**	**1 0 1**
30.94	4.24	2.8905	0 1 2
33.13	10.19	2.7039	1 0 4
34.70	**45.17**	**2.5855**	**0 1 5**
38.60	27.72	2.3327	1 0 7
40.87	**99.75**	**2.2079**	**0 1 8**
45.95	19.23	1.9749	1 010
48.72	5.54	1.8689	0 111
51.74	1.73	1.7667	0 015
53.59	**54.80**	**1.7100**	**1 1 0**
54.66	18.45	1.6792	1 013
62.84	2.76	1.4787	1 1 9
62.85	3.32	1.4786	0 2 1
63.15	6.79	1.4722	0 018
64.46	6.55	1.4456	1 016
64.47	1.00	1.4452	0 2 4
65.44	5.08	1.4263	2 0 5
67.97	3.81	1.3791	0 2 7
69.53	15.29	1.3519	2 0 8
73.22	3.57	1.2927	0 210

Notes: The most intense calculated diffraction reflections are shown in bold. X-ray wavelength: 1.541838. Bounds on 2θ: 0.0 75.0. Limits imposed on the indices are: ±2 ±2 ±20. Max. abs. intensity/volume**2: 40.14456934 .The intensity cut-off value is 1.00. XPOW (Downs et al. 1993).

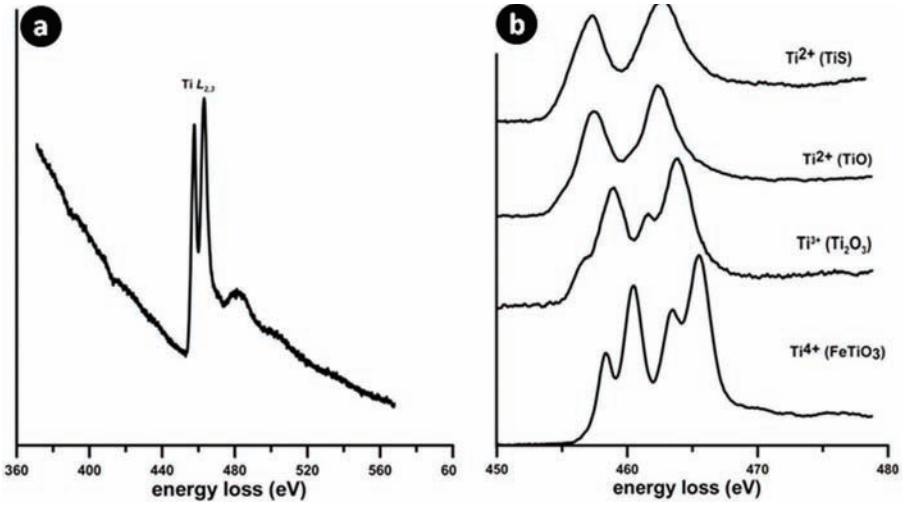

FIGURE 4. EELS spectra of wassonite. (**a**) EELS spectra acquired from wassonite grain 1 showing no nitrogen (400–420 eV) or oxygen (530–550 eV) signal, thus excluding the presence of titanium nitride or oxide. (**b**) EELS spectra of Ti $L_{2,3}$-edge structure from wassonite grain 1 and reference materials. Titanium valence proved to be divalent in wassonite.

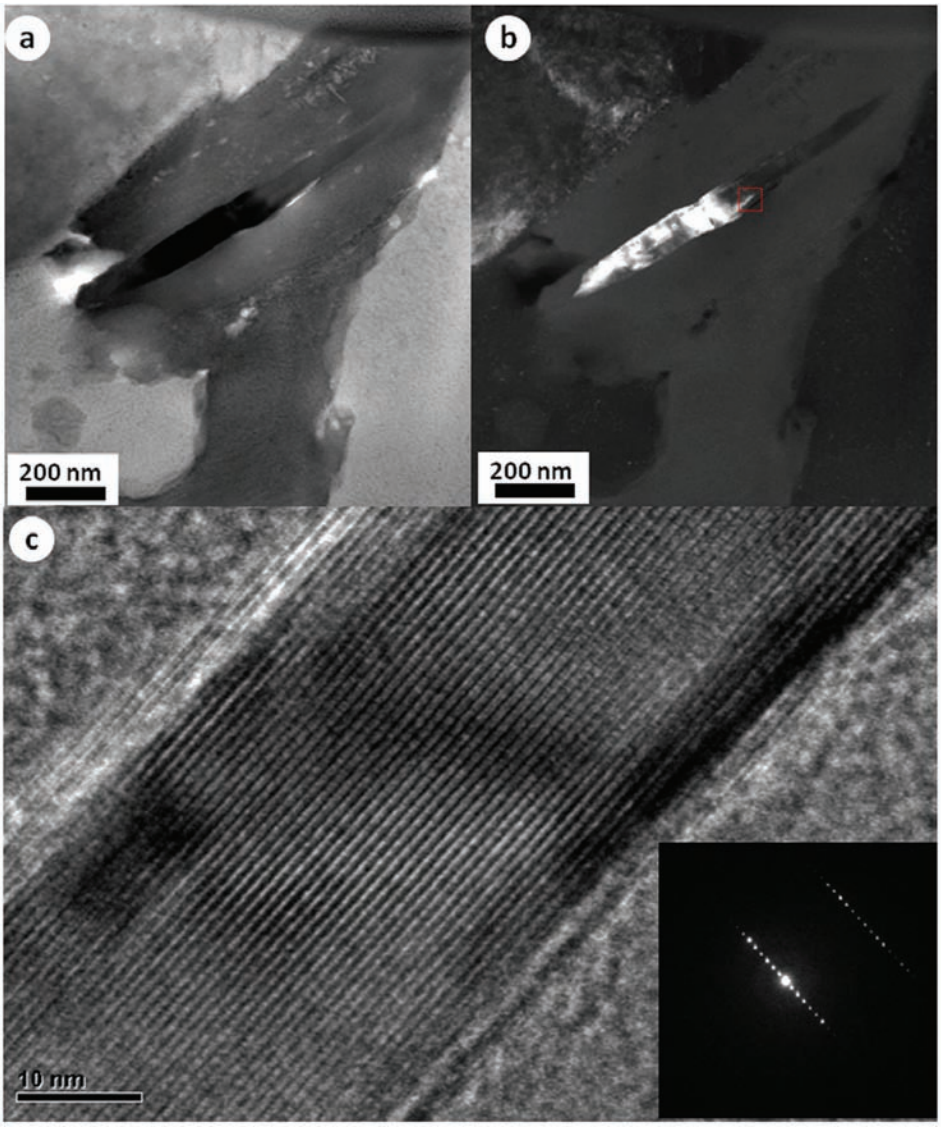

FIGURE 5. Wassonite grain 1 is a single crystal. (**a**) A bright-field STEM micrograph showing wassonite grain 1 in dark contrast. Note that this image is taken from a different tilting than Figure 3, so that the contrast of wassonite grain 1 is different. (**b**) A high-angle annular dark-field (HAADF) STEM micrograph of the same angle of **a**. (**c**) A high-resolution TEM micrograph of wassonite grain 1 from the boxed area in **a**. Inset is the selected-area electron diffraction (SAED) pattern of wassonite from the same tilting.

to the cooling rate (Jacquinn and Jeannin 1963). TiS tends to be the R9 type rather than the NiAs type when cooled slowly from 1200 °C in water (Mitsui 2003). When the original melting *T* is low (800 to 1000 °C), all of the TiS tends to become R9-type no matter how fast the cooling rate (Mitsui 2003).

Physical and optical properties of wassonite

Optical properties are not measurable using the available samples and no data have been found in the literature. Color is dark bronze to brown for synthetic TiS (Strotzer et al. 1939). The Vickers hardness number VHN_{100} = 580 kg/mm^2 for synthetic TiS material (Samsonov and Drozdova 1972).

DISCUSSION

Titanium monosulfide has been synthesized and studied by materials scientists for decades, but it has never before been found in nature. Its discovery in the Y 691 enstatite chondrite makes wassonite the first new monometallic sulfide mineral described in more than four decades and the first binary monosulfide known among group-IVB elements (CAS system). Other binary monosulfides include AsS (realgar), CaS (oldhamite), CdS (greenockite; hawleyite), CuS (covellite), FeS (troilite), HgS (cinnabar), MgS (niningerite), MnS (alabandite; rambergite), NiS (millerite), PbS (galena), PdS (vysotskite), PtS (cooperite),

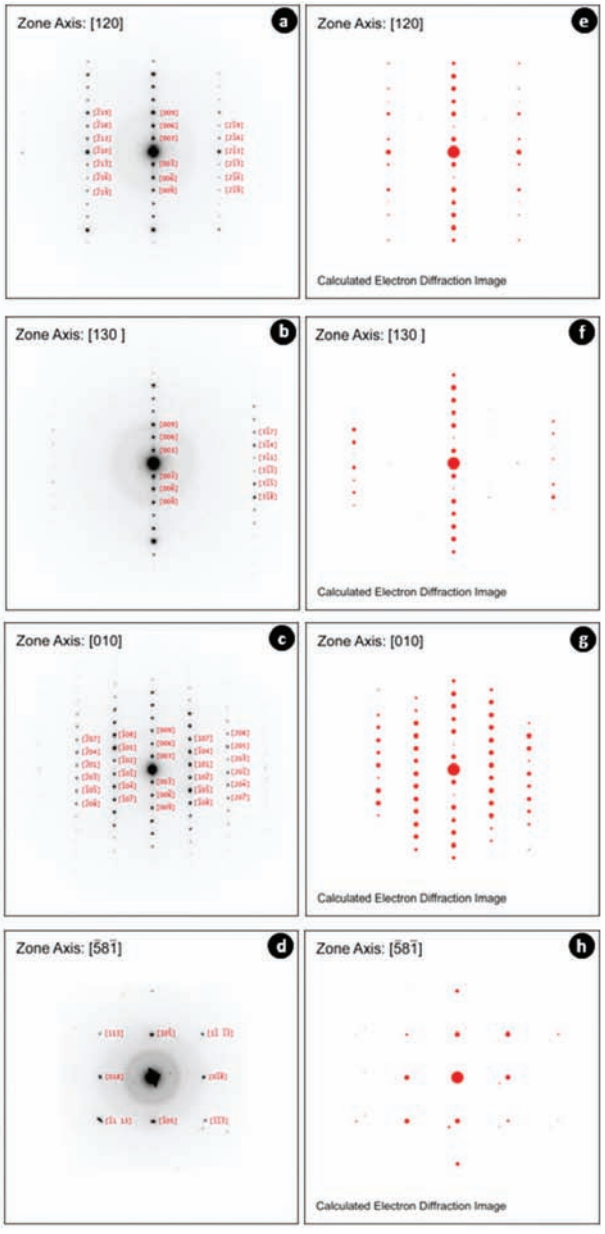

FIGURE 6. Crystallography of wassonite. (**a**–**d**) SAED patterns from wassonite grain 1 with 4 different zone axes. (**e**–**h**) Computer-simulated SAED patterns from synthetic rhombohedral TiS corresponding to each measured SAED condition of wassonite.

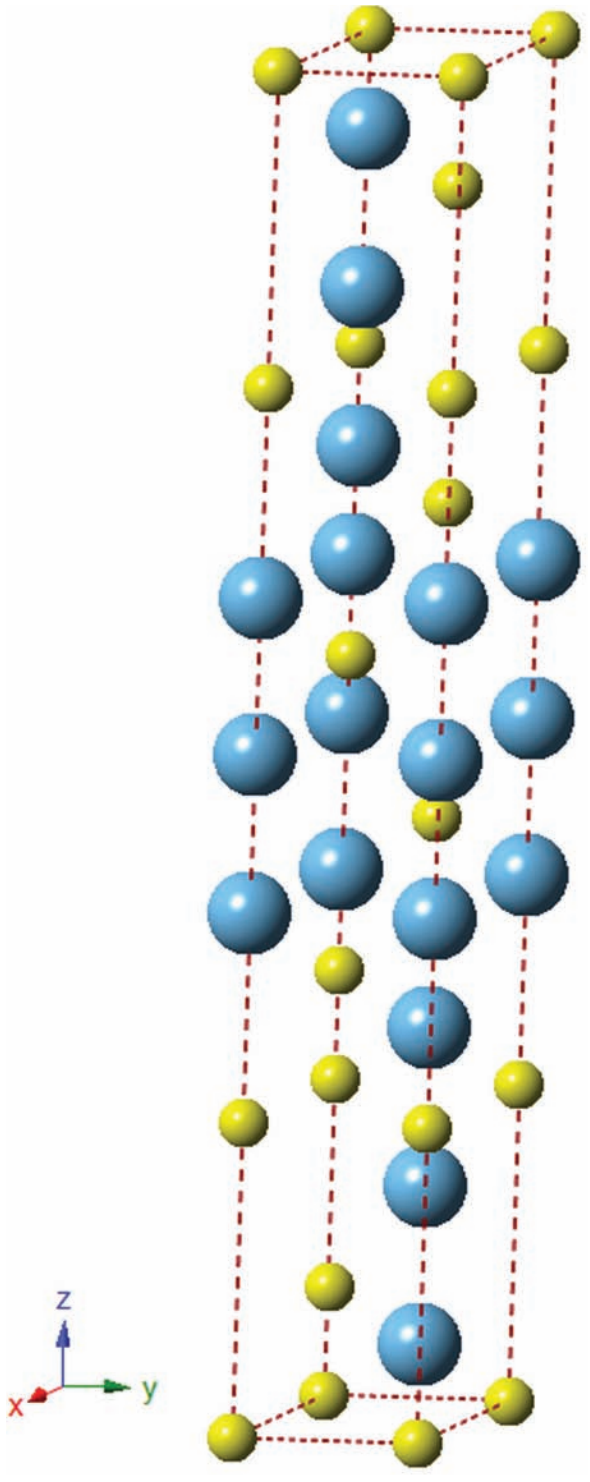

FIGURE 7. Wassonite crystal unit cell. Blue = Ti, yellow = S.

SnS (herzenbergite), and ZnS (sphalerite; wurtzite; matraite). It seems likely that additional binary monosulfides (e.g., BaS, BeS, CoS, CrS, GaS, SrS, and VS) that exist as synthetic compounds will one day be identified in reduced meteorites or low-oxygen-fugacity terrestrial ore deposits as naturally occurring phases.

Titanium shows partial chalcophile behavior in enstatite-rich meteorites. Previous occurrences of Ti-bearing sulfides in enstatite chondrites and enstatite achondrites (aubrites) include troilite (up to 0.95 wt% Ti in enstatite chondrites and up to 16 wt% Ti in aubrites), daubréelite (up to 0.25 wt% Ti in enstatite chondrites and up to 0.22 wt% Ti in aubrites), niningerite (up to 0.09 wt% Ti in enstatite chondrites), oldhamite (up to 0.02 wt% in enstatite chondrites), and ferroan alabandite (up to 0.04 wt% Ti in enstatite chondrites and up to 0.10 wt% Ti in aubrites) (Keil 1968, 1969), as well as heideite $(Fe,Cr)_{1+x}(Ti,Fe)_2S_4$ with

28.5 wt% Ti in the Bustee aubrite (Keil and Brett 1974). The new mineral wassonite is the Ti-rich end-member of the monosulfide group. Until recently, no titanium sulfides were known to occur naturally. However, there is a report of an unnamed mineral UM2007-31-S:Ti, Unnamed 2656 (Smith and Nickel 2007) that has the composition Ti_7S_3 as does another titanium-dominant sulfide.

Origin of wassonite

Wassonite was discovered in a BO chondrule within the Yamato 691 EH3 chondritic meteorite. Like all other chondrules in chondritic meteorites, BO chondrules are thought to have formed in the solar nebula by melting fine-grained precursor dust (e.g., Rubin 2000; Jones et al. 2005). BO chondrule textures develop after complete melting of a solid olivine-normative precursor assemblage. Because chondrules in different chondrite groups have different O-isotopic compositions (e.g., Fig. 10 of Jones et al. 2005), it seems likely that chondrules formed locally in the nebula. Thus, this BO chondrule and the wassonite grains within it presumably formed in the same location where the EH asteroid accreted. This is likely to have been in the inner solar system. Enstatite chondrites probably formed inside the orbit of Mars, perhaps at a distance of ~1 AU or less from the Sun (Wasson 1985, 1988). The Cr-, Ni-, and Ti-isotopic compositions of enstatite chondrites are similar to those of Earth (Trinquier et al. 2007, 2009; Regelous et al. 2008) and their O- and N-isotopic compositions are similar to those of Earth and Mars (e.g., Clayton 1993; Javoy 1995; Mohapatra and Murty 2003).

The phases in the BO chondrule are highly reduced and indicate formation at low oxygen fugacities. The precursor of the chondrule may have included fine-grained magnesian olivine, amorphous feldspathic material, Ti-bearing troilite, metallic Fe-Ni, and possibly graphite. During melting, the chondrule probably reached temperatures ≥1900 K and then quenched by radiation. Two melts coexisted in the chondrule precursor—a silicate melt and an Fe-FeS melt. Under the reducing conditions present in enstatite chondrites, substantial amounts of S can partition from the Fe-FeS melt into the coexisting silicate melt (Fogel 1997). Up to 8 wt% S has been observed experimentally in melts produced from enstatite chondrites (Fogel et al. 1996; McCoy et al. 1999). Partitioning of substantial S into the silicate melt raised the Ti concentration in the residual Fe-FeS melt. By the time sulfide crystallized from this melt, the Ti concentration was high enough to form small grains of wassonite. Other opaque phases crystallizing from the melt included kamacite and troilite. Olivine bars formed from the silicate melt during quenching. Reduced Ti is unlikely to have partitioned into the metal. Although kamacite in enstatite chondrites can contain several weight percent Si (e.g., Keil 1968), Ti is apparently more difficult to reduce to the metallic state than Si; thus, the Ti concentration in meteoritic metal is very low. Some Ti^{2+} occurs in olivine and glassy mesostasis (Table 1), but sufficient amounts were available to also partition into wassonite (Table 2). Using mass-balance estimates (and compositions listed in Table 2), we deduce that ~40% of the Ti in the BO chondrule occurs in wassonite, ~35% in mesostasis, ~25% in olivine, and ~1% in other phases (troilite, osbornite, schöllhornite, and the as-yet-undescribed Ti-rich layer phases).

Wasson (1996) noted that volatile elements such as Na and S occur in chondrules in their cosmic proportions. Thus, chondrules were not appreciably devolatilized and could not have been heated above 1000 K for longer than ~100 s. This corresponds to a mean cooling rate exceeding 30 000 °C/h. This scenario is consistent with the results from synthetic TiS polymorph studies.

It seems plausible that additional grains of wassonite could be found in droplet chondrules (i.e., radial pyroxene, cryptocrystalline, and barred olivine types) in EH3 and EL3 chondrites. It is even possible that relatively coarse grains might occur as phenocrysts in aubrites.

We are planning to measure the O isotopes of olivine bars and the Al-Mg isotopic system of the mesostasis from the wassonite-containing BO chondrule using the NanoSIMS 50L at NASA Johnson Space Center, which may help to constrain the origin of this unusual phase.

Acknowledgments

This paper benefitted from helpful comments by Chi Ma, Klaus Keil, an anonymous reviewer, and associate editor Rhian Jones. We thank the JARE-10 team for their life-risking expedition to collect Antarctic meteorites including Yamato 691. We thank NIPR for preparing and loaning the specimen. We are grateful to John Wasson for allowing us to use his name for this new mineral. The JEOL 2500 SE field-emission STEM was obtained through a grant from the NASA SRLIDAP program. This work was supported by NASA Cosmochemistry grants NNG06GF95G (A.E.R.), NNH10ZDA001N (K.N.-M., L.P.K.), and Korean NRFMEST grant 2011-0027574 (B.-G.C.).

References cited

Clayton, R.N. (1993) Oxygen isotopes in meteorites. Annual Review of Earth and Planetary Sciences, 21, 115–149.

Clayton, R.N., Mayeda, T.K., and Rubin, A.E. (1984) Oxygen isotopic compositions of enstatite chondrites and aubrites. Proceedings of Lunar and Planetary Science Conference, 15, C245–C249.

Cliff, G. and Lorimer, G.W. (1975) The quantitative analysis of thin specimens. Journal of Microscopy, 103, 203–207.

Downs, R.T., Bartelmehs, K.L., Gibbs, G.V., and Boisen, M.B. Jr. (1993) Interactive software for calculating and displaying X-ray or neutron powder diffractometer patterns of crystalline materials. American Mineralogist 78, 1104–1107.

Fogel, R.A. (1997) The enstatite chondrite-achondrite link reforged: Solution of the titanium in troilite problem (abstract). Meteoritical and Planetary Science, 32, A43.

Fogel, R.A., Weisberg, M.K., and Prinz, M. (1996) The solubility of CaS in aubritic silicate melts (abstract). Lunar and Planetary Science, 27, 371–372.

Gaffey, M.J. and Kelley, M.S. (2004) Mineralogical Variations among high albedo E-type asteroids: Implications for asteroid igneous processes. Lunar and Planetary Science XXXV, 1812.

Grossman, J. (1995) Meteoritical Bulletin Database Version 7.1, issued by the Meteoritical Society, Chantilly, Virginia.

Harn, V.H., and Harder, B. (1956) Zur Kristallstructur der Titansulfide. Zeitschrift fuer anorganische und allgemeine Chemie, 288, 241–348.

Jacquinn, Y. and Jeannin, Y. (1963) The titanium-sulfur system near the composition TiS. Comptes Rendus, 256, 5362–5365.

Javoy, M. (1995) The integral enstatite chondrite model of the earth. Geophysical Research Letters, 22, 2219–2222.

Jones, R.H., Grossman, J.N., and Rubin, A.E. (2005) Chemical, mineralogical and isotopic properties of chondrules: clues to their origin. In A.N. Krot, E.R.D. Scott, and B. Reipurth, Eds., Chondrites and the Protoplanetary Disk, 341, p. 251–285. ASP Conference Series, Astronomical Society of the Pacific, Orem, Utah.

Keil, K. (1968) Mineralogical and chemical relationships among enstatite chondrites. Journal of Geophysical Research, 73, 6945–6976.

——— (1969) Titanum distribution in enstatite chondrites and achondrites, and its bearing on their origin. Earth and Planetary Science Letters, 7, 243–248.

Keil, K. and Brett, R. (1974) Heideite $(Fe, Cr)_{1+x}(Ti, Fe)_2S_4$, a new mineral in the Bustee enstatite achondrite. American Mineralogist, 59, 467–470.

Kojima, H. (2006) The history of Japanese Antarctic meteorites. In G.J.H. McCall, A.J. Bowden, and R.J. Howarth, Eds., The History of Meteoritics and Key Meteorite Collections: Fireballs, Falls and Finds, 256, p. 291–304. Geological Society Special Publication, Boulder, Colorado.

McCoy, T.J., Dickinson, T.L., and Lofgren, G.E. (1999) Partial melting of the

Indarch (EH4) meteorite: A textural, chemical and phase relations view of melting and melt migration. Meteoritics & Planetary Science, 34, 735–746.
Mitsui, H. (2003) Phase stability and microstructural control of CrS, TiS and $Ti_4C_2S_2$ in alloys. Ph.D. thesis, Tohoku University, Sendai, Japan.
Mitsui, H., Sasaki, T., Oikawa, K., and Ishida, K. (2009) Phase Equilibria in FeS-XS and MnS-XS (X=Ti, Nb and V) Systems. Journal of the Iron and Steel Institute of Japan, 49, 936–941.
Mohapatra, R.K., and Murty, S.V.S. (2003) Precursors of Mars–Constraints from nitrogen and oxygen isotopic compositions of martian meteorites. Meteoritics & Planetary Science, 38, 225–242.
Nolze, G. and Kraus, W. (1998) PowerCell 2.0 for Windows. Powder Diffraction, 13, 256–259.
Palmer, D. (2005) SingleCrystal for Windows software version 1.0.2 designed by David Palmer. CrystalMaker Software, Oxfordshire, U.K.
Regelous, M., Elliott, T., and Coath, C. (2008) Nickel isotope heterogeneity in the early Solar System. Earth and Planetary Science Letters, 272, 330–338.
Rubin, A.E. (2000) Petrologic, geochemical and experimental constraints on models of chondrule formation. Earth Science Reviews, 50, 3–27.
Samsonov, G.V. and Drozdova, S.V. (1972) Sulfidy [in Russian], Metallurgiya, Moscow, vol. 4, table 41 in Handbook for Sulfides, Japanese, p. 115–125.
Smith, D.G.W. and Nickel, E.H. (2007) A system for codification for unnamed minerals: report of the Subcommittee for Unnamed Minerals of the IMA Commission on New Minerals, Nomenclature and Classification. Canadian Mineralogist, 45, 983–1055.
Strotzer, E.F., Biltz, W., and Meisel, K. (1939) Zirkoniumsulfide. Zeitschrift für anorganische und allgeneine Chemie, 242, 249–271.
Trinquier, A., Bizzarro, M., Ulfbeck, D., Krot, A.N., and Connelly, J.N. (2007) Origin of titanium isotope heterogeneity in the protoplanetary disk. Workshop on the Chronology of Meteorites and the Early Solar System, November 5–7, 2007, Kauai, Hawaii. LPI Contribution 1374, 171–172.
Trinquier, A., Elliott, T., Ulfbeck, D., Coath, C., Krot, A.N., and Bizzarro, M. (2009) Origin of nucleosynthetic isotope heterogeneity in the solar protoplanetary disk. Science, 324, 374–376.
Wasson, J.T. (1985) Relationships between chondritic meteorites and planets. Lunar and Planetary Institute Terrestrial Planets: Comparative Planetology, p. 1.
——— (1988) The building stones of the planets. In F. Vilas, C.R. Chapman, and M.S. Matthews, Eds., Mercury, p. 622–650. University of Arizona Press, Tucson.
——— (1996) Chondrule formation: Energetics and length scales. In R.H. Hewins, R. Jones, and E.R.D. Scott, Eds., Chondrules and the Protoplanetary Disk, p. 45–55. Cambridge University Press, U.K.
Wasson, J.T., Kallemeyn, G.W., and Rubin, A.E. (1994) Equilibration temperatures of EL chondrites: A major downward revision in the ferrosilite contents of enstatite. Meteoritics, 29, 658–662.
Weisberg, M.K., McCoy, T.J., and Krot, A.N. (2006) Systematics and evaluation of meteorite classification. In D.S. Lauretta and H.Y. McSween, Eds., Meteorites and the Early Solar System II, p. 19–52. University of Arizona Press, Tuscon.

MANUSCRIPT RECEIVED JULY 12, 2011
MANUSCRIPT ACCEPTED JANUARY 4, 2012
MANUSCRIPT HANDLED BY RHIAN JONES

APPENDIX 1

The TEM stage orientation for each zone axis can be related to another via the respective X and Y tilts of the sample stage necessary to bring the given zone axis parallel to the TEM electron beam. If α and β represent the respective X and Y tilts of a given zone axis then the unit vector defining sample normal orientation with respect to the laboratory reference frame (i.e., [001] vertical) is given by the following expression:

$$\langle i, j, k \rangle = \begin{bmatrix} \sin(\alpha) \\ \sin(\alpha) \cdot \quad \sin(\beta) \\ \sin(\alpha) \cdot \quad \sin(\beta) \end{bmatrix}.$$

Thus, we can visualize the spatial relationships between the observed zone axes by plotting the projection of the unit vectors, defining the sample orientations corresponding to each zone axis, on to an origin-centered sphere as shown. To help with the interpretation, we re-centered and rotated the projection so that zone axis "7" is in the center, the blue point marked "+" representing the original center. Any set of points that lie on the same longitudinal line are related by rotation about a common axis. In the plot it can be seen that zone axes "7", "9", and "8" all lie on the prime meridian with latitudes of 0, ~19, and ~30°, respectively. Hence these zone axes are related by a common rotation. This is consistent with their assignment as the [010], [130], and [120] zone axes of an $R\bar{3}m$ unit cell, in which the common rotation is about the *c* axis and the calculated angles between the zone axes [010] ∧ [130] and [010] ∧ [120] are 19.1 and 30.0°, respectively.

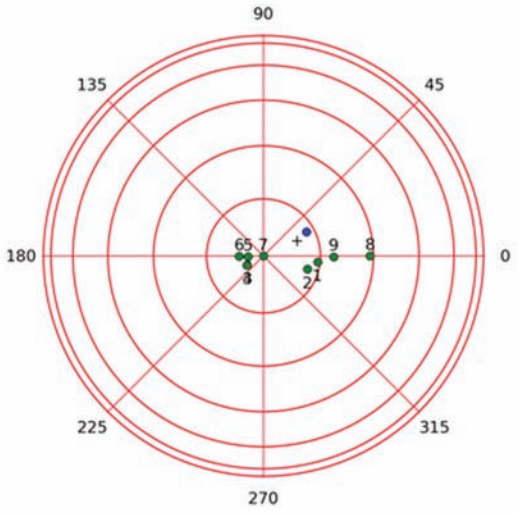

APPENDIX FIGURE 1. Stereographic projection representing the nine observed zone axes.